2022

# Energy savings of radiative cooling paints applied to residential buildings

J. Peoples

Y.-W. Hung

Z. Fang

J. Braun

W. T. Horton


*See next page for additional authors*

## Authors

J. Peoples, Y.-W. Hung, Z. Fang, J. Braun, W. T. Horton, and X. Ruan

# Energy savings of radiative cooling paints applied to residential buildings

Joseph Peoples [a,1], Yu-Wei Hung [b,1], Ziqi Fang [a], James Braun [a], W. Travis Horton [b,*], Xiulin Ruan [a,*]

[a] School of Mechanical Engineering, Purdue University, West Lafayette, IN 47907, USA
[b] School of Civil Engineering, Purdue University, West Lafayette, IN 47907, USA

## ARTICLE INFO

## ABSTRACT

There is a growing need to understand the real-world utility and potential energy savings of radiative cooling (RC) materials. Here, we present a high-fidelity RC model which accounts for pertinent weather factors including: precipitable water, sky clearness, and dynamic convective heat transfer coefficients based on wind speed. We implement our RC model on a single-story residential building to study the impact of RC in all the ASHRAE climate zones in the United States using the 16 DOE recommended representative cities for each climate zone. For each city, we model two building types to explore both the retrofit implementation of RC materials on a typical building in use today, as well as future buildings integration based on the high efficiency building recommendations provided by the DOE. Our results show >7% and >12% electricity savings across the United States for the high efficiency building and typical building, respectively. Interestingly, we find the main benefit comes from the material's ability to offset solar gains, while the heat flux from cooling the exterior surface temperature below the ambient is a secondary benefit. Furthermore, warm climates yield the greatest electricity savings of up to 22% and 46% for the high efficiency and typical building, respectively. We observed that warm climates utilize the "full effects" of RC materials as the below ambient cooling of the exterior is sufficient cooling to lower the interior below the set-point temperature, which greatly reduces the cooling energy demand.

## 1. Introduction

Cooling homes with conventional air conditioning techniques is both costly and not environmentally friendly. If the cooling demand for residential homes was decreased by as little as 1% across the United States, it would correlate to an annual decrease of 118 thousand metric tons of carbon dioxide emissions from electricity production [1]. Radiative cooling is a passive, sustainable cooling method that utilizes deep-space as an infinite heat sink at a constant 3 K where heat can be rejected through the highly transparent region of the atmosphere, from 8 - 13 μm, known as the "sky-window". Many studies have investigated the adaptation of radiative cooling as either a complete alternative or a retrofit efficiency gain to existing air conditioning. However, they did not include the comprehensive effects of dynamic convective heat loads due to wind, cloud coverage, or the atmospheric transmittance de-

crease due to humidity which all have major impacts on the cooling performance of radiative cooling technologies.

Over the last several years the field of passive radiative cooling has exploded with novel new materials that have shown 24 h cooling, even when exposed to direct solar irradiation [2–4]. With these advancements on the materials side, the field would benefit from feasibility studies of real-world implementation of these passive radiative coolers to offset cooling demands. There have been multiple studies on utilizing modular radiative cooling systems for large-scale cold plates and incorporating the cooled working fluid into an air conditioning cycle to estimate energy savings, as well as incorporating radiative cooling films as standalone roofing materials [5–9]. Other studies have investigated the effects of certain weather parameters, such as humidity or ambient temperature, on the cooling power of radiative cooling surfaces and their respective energy savings [6,10–12]. Moreover, there have been several works on creating building materials, such as engineered wood, paper, and bulk fire retardant, with radiative cooling characteristics for sustainable, energy efficient buildings in the future [13–16]. Recently, radiative cooling paints have been of interest due to their scalabilty, cost, and ease of implementation [17–19]. Earlier stud-

* Corresponding authors.
*E-mail addresses:* wthorton@purdue.edu (W.T. Horton), ruan@purdue.edu (X. Ruan).
[1] Equal Contributions

ies, which share a subset of authors with the current work, have demonstrated two radiative cooling paints with 24 h cooling performance [20–22]. However, they did not evaluate the energy savings that are possible if these materials are retrofitted onto existing buildings. All these studies motivate the need for a more complete understanding of the benefits radiative cooling can provide, in terms of annual energy savings, across all United States climate zones.

Here, we have coupled a novel radiative cooling model with a high-fidelity building envelope simulation to more accurately depict the benefits of utilizing exterior radiative cooling surfaces on all parts of the building. The increase in the fidelity of our model comes from the treatment for dynamic convective loads due to wind speed, decreases in atmospheric transmittance due to precipitable water (i.e. humidity), accounting for cloud coverage, and variable solar irradiation intensity. We model the impact of radiative cooling surfaces on both a prototypical single story residential building and a National Renewable Energy Laboratory (NREL) high efficiency single story residential building. We simulate a typical cooling season for each DOE recommended representative city for every ASHRAE climate zone in the United States, utilizing the previously mentioned weather parameters, and we present the cooling energy savings of radiative cooling for each climate zone [23,24].

## 2. Methods

### 2.1. Building envelope model

The building model is constructed based on a single-story, rectangular ranch style residential with two doors and six windows, developed by Holloway [25]. Holloway constructed the building model in TRNSYS based upon a high fidelity residential building model proposed by Smith et al. [24,25]. TRNSYS is a dynamic building simulation software, developed by the Thermal Energy System Specialists and the University of Wisconsin Solar Energy Laboratory, and it is utilized to calculate the building energy performance and HVAC system power consumption in this study [26].

The ranch style building is an 1800 ft$^2$, 1-story residence [25]. The building envelopes of Holloways design are established according to Smiths analysis. However, the envelopes were modified with higher thermal resistance (R-39, 13-3/4g roof; R-25, 9-1/2g exterior walls) for greater efficiency [24,25]. This high efficiency ranch style building will be referred to as the High-Efficiency Building in this work moving forward. However, these thermal resistances are not common for existing residential buildings. Since our radiative cooling paint is ideal for retrofitting existing buildings to increase their energy efficiency, we modeled a more typical ranch style building. This model was constructed based on a typical range of building envelopes (R-18, 6g roof; R-11, 4g exterior walls) and will be referred to as the Typical Building in this work moving forward. The HVAC system utilized in both the High-Efficiency and Typical Buildings is based on a constant air volume design. In this study, the cooling is provided by a single-speed air conditioner based on TRNSYS's built-in single-speed air-conditioner (AC) module (Type 921) and the cooling set-point temperature is 23 °C. The power consumption of the AC ($P_{AC}$) is proportionally calculated according to,

$$P_{AC} = P_{921} \frac{Q_{sen}}{Q_{921}} \tag{1}$$

which is the instant A/C power consumption output from Type 921 provided in TRNSYS library, ($P_{921}$), the sensible load of the space ($Q_{sen}$), and sensible heat removal rate provided by Type 921 ($Q_{921}$) [26]. The internal gains schedule is assigned based on ASHRAE 90.2, and the infiltration rate schedule was from ASHRAE 62.2

[27,28]. Table 1 has the specifics for each type of building utilized in this work [25].

The RC solar absorptance and mid-IR emittance represent values somewhat similar to that of the novel RC paints [21,22,29]. The view factors of the building to the sky were conservatively assumed to be 0.9 for the roof to account for another building or trees in the area and 0.4 for the walls based on the height to width ratio of the building walls using Table 13-1 in Cengel's text [30].

The energy consumption reduction of applying the radiative cooling paint on all exterior surfaces of a building is investigated. The ranch style residential building will illustrate the maximum benefit from radiative cooling since the roof area relative to the volume is large and directly tied to the air conditioned space. The radiative cooling (RC) paint is factored into the TRNSYS model as an external heat flux on the exterior building surfaces. The RC paint heat flux is depended on weather parameters and surface temperature and will be discussed further in Radiative Cooling Model section.

A dynamic forced convective heat transfer coefficient was implemented for the exterior surfaces of the building model to deliver simulations closer to reality. It was calculated by [31],

$$h_c = 12.12 - 1.16 V_w + 11.6 V_w^{0.5} \tag{2}$$

where $V_w$ is the wind velocity. Note that this correlation is valid from 2 to 20 m/s. To gain an extensive understanding of the benefits of the RC paint in a diverse range of climates, we utilize the DOE's 16 recommended cities for each type of ASHRAE climate zone, shown in Table 2 [23,32]. The weather data sets of the target cities were obtained from the typical meteorological year (TMY3) files published by the United States Department of Energy, and the study period is focused on the summer months, i.e. cooling season (May 1st, 12 AM to October 1st, 12 AM) [33].

### 2.2. Radiative cooling model

To accurately predict the amount of heat rejected from a radiative cooling surface, more weather parameters need to be considered compared to traditional building envelope models. Our model introduces two terms to the traditional radiative cooling power calculations: $\beta$ which is the sky clearness factor and $\varepsilon_{atm}(PW, \lambda)$ which is the atmospheric emittance that is dependent on the precipitable water, $PW$, and the wavelength, $\lambda$. Precipitable water is an absolute measure of water vapor content in the air. If one were to take a column of air from the earth's surface to the upper atmosphere and condense all the water vapor within that column, it would have some height associated with it. This height is referred to as the precipitable water and is measured in mm [34]. The precipitable water can be related to the relative humidity, given the ambient temperature and pressure; however, this work will present all results in terms of precipitable water as it is an absolute measure of water content which directly impacts the atmospheric transmittance/emittance.

To calculate the thermal radiation, $P_{rad}$, for our radiative cooling surface we first calculate the amount of thermal radiation leaving the surface, $P_{LWR}$, given by,

$$P_{LWR}(T_s) = \int_0^{\pi/2} \int_0^{\infty} 2\pi \sin(\theta) \cos(\theta) I_{bb}(T_s, \lambda) \varepsilon_s(\lambda, \theta) \, d\lambda \, d\theta \tag{3}$$

$$I_{bb}(T, \lambda) = \frac{2\hbar c_0^2}{\lambda^5 \left[ exp\left( \frac{\hbar c_0}{\lambda T k_B} \right) - 1 \right]} \tag{4}$$

where $T_s$ is the surface temperature, $\varepsilon_s(\lambda, \theta)$ is the emissivity of the surface, and $I_{bb}$ is the black body spectral intensity calculated with Planck's constant, $\hbar$, the speed of light in vacuum, $c_0$, and

**Table 1**
Pertinent building model parameters.

| Parameter | High-Efficiency Building | Typical Building |
|---|---|---|
| Conditioned Floor Area [m$^2$] | 167.2 | |
| Building Volume [m$^3$] | 407.8 | |
| Wall Area (fron/side) [m$^2$] | 537.7/23.4 | |
| Total Window Area (front/side) [m$^2$] | 8.1/3.4 | |
| Roof Area (front/side) [m$^2$] | 90.5/15.1 | |
| Door Area [m$^2$] | 2.1 | |
| Roof U-Value [W/m$^2$K] | 0.145 | 0.305 |
| Wall U-Value [W/m$^2$K] | 0.229 | 0.486 |
| Roof Emissivity at 10 μm (no RC/RC) [-] | 0.92/0.92 | |
| Wall Emissivity at 10 μm (no RC/RC) [-] | 0.92/0.92 | |
| Door Emissivity at 10 μm (no RC/RC) [-] | 0.90/0.92 | |
| Roof Total Solar Absorptivity (no RC/RC) [-] | 0.70/0.036 | |
| Wall Total Solar Absorptivity (no RC/RC) [-] | 0.70/0.036 | |
| Door Total Solar Absorptivity (no RC/RC) [-] | 0.60/0.036 | |
| View Factor (roof/side) [-] | 0.90/0.50 | |

**Table 2**
DOE recommended representative cites for every climate zone in the United States [23].

| ASHRAE Climate Zone | Description | Representative City |
|---|---|---|
| 1A | Very Hot, Humid | Miami, FL |
| 2A | Hot, Humid | Houston, TX |
| 2B | Hot, Dry | Phoenix, AZ |
| 3A | Warm, Humid | Atlanta, GA |
| 3B-Coast | Warm, Marine | Los Angeles, Ca |
| 3B | Warm, Dry | Las Vegas, NV |
| 3C | Warm, Marine | San Francisco, CA |
| 4A | Mild, Humid | Baltimore, MD |
| 4B | Mild, Dry | Albuquerque, NM |
| 4C | Mild, Marine | Seattle, WA |
| 5A | Cold, Humid | Chicago, IL |
| 5B | Cold, Dry | Boulder, CO |
| 6A | Cold, Humid | Minneapolis, MN |
| 6B | Cold, Dry | Helena, MT |
| 7A | Very Cold | Duluth, MN |
| 8A | Sub-Arctic | Fairbanks, AK |

Boltzmann's constant, $k_B$ [35,36]. Then we calculate the amount of thermal irradiation coming from the atmosphere and absorbed by the surface, $P_{atm}$, using

$$P_{atm}(T_{amb}, PW) = \int_0^{\pi/2} \int_0^{\infty} 2\pi \sin(\theta) \cos(\theta) I_{bb}(T_{amb}, \lambda)$$
$$\times \varepsilon_s(\lambda, \theta) \varepsilon_{atm}(\lambda, \theta, PW) \, d\lambda \, d\theta \qquad (5)$$

where $T_{amb}$ is the ambient temperature and $\varepsilon_{atm}(\lambda, \theta, PW)$ is the atmospheric emittance that is dependent on the precipitable water, $PW$. Though there are other molecules in our atmosphere that cause absorptance in the mid-infrared spectral region, water vapor has strong absorptance due to the H-O-H bonds and the size and quantity of the water molecules in the atmosphere [34]. A free online platform, MODTRAN, shows the atmospheric transmittance as a function multiple variables, including the water column, $WC$ [37–39]. Precipitable water can be converted to the water column with the atmospheric pressure, molar density of water and specific volume. We assume the atmospheric transmittance is independent of temperature within temperature range of approximately -100 °C and 50 °C, as the majority of the molecules in the atmosphere, nitrogen, oxygen, and water have weak temperature dependent optical responses from 8 to 13 μm within the specified temperature range [40–43]. Once we have calculated the net thermal long wave radiation, we determine the amount of absorbed power due to solar irradiation, $P_{solar}$, using,

$$P_{solar}(PW) = \int_0^{\infty} I_{solar}(\lambda, PW) \varepsilon_s(\lambda) \, d\lambda \qquad (6)$$

where $I_{solar}(\lambda, PW)$ is the solar intensity which is dependent on the precipitable water as well, due to the O-H bonds having strong absorptance peaks in the 2–3 μm range, and higher order molecular interactions causing absorptance peaks at shorter wavelengths [34]. Lastly, we calculate the net radiation leaving the surface, $P_{rad}$, by,

$$P_{rad} = \beta[P_{LWR}(T_s) - P_{atm}(T_{amb}, PW)] - P_{solar}(PW) \qquad (7)$$

where the sky clearness factor, $\beta$, accounts for cloud coverage, e.g. $\beta = 1 - 0.22 = 0.78$ if there is 22% cloud cover in the atmosphere. The TMY3 data set provides the sky clearness factor for most cities [33]. It should be noted that this treatment of the sky clearness is conservative as we do not account for any blocking of the solar irradiation; however, the TMY3 data set should account for some of the cloud coverage effects in their solar irradiation measurements.

## 3. Results

### 3.1. Impact of precipitable water and sky clearness

To illustrate the impact of precipitable water (PW) on radiative cooling performance we collected the atmospheric transmittance from 2.5 to 20 μm varying the PW from 0 to 60 mm at an interval of 2 mm using MODTRAN's online tool [37–39]. From the 40 spectral atmospheric transmittance profiles, we linearly interpolated the data to be a 1 mm PW resolution and this data is shown in Fig. 1(a). The atmospheric transmittance from 8 to 13 μm (the sky-window) shows a strong dependence on precipitable water which correlates to a decrease in radiative cooling power with an increase in PW. From Fig. 1a, we can calculate the irradiation from the atmosphere, $P_{atm}$, using Eq. 5. Fig. 1(b) shows the atmospheric irradiation with respect to PW and ambient temperature.

Figs. 1 (a) and 1(b) elucidate a deeper understanding of the humidity dependence on radiative cooling; as the PW, i.e. humidity, increases the atmospheric transmittance decreases, decreasing the thermal energy rejected to deep-space which is an infinite heat sink at 3 K. The atmospheric irradiation increases due to the water molecules absorptance. These coupled effects lead to decrease in the net cooling power any radiative cooling surface can achieve regardless of their solar reflectance or mid-IR emittance.

The radiative cooling power of the RC paint, $P_{rad}$, can be calculated with a given solar irradiation value, $P_{solar}$, and a sky clearness, $\beta$. To illustrate the dependence of the PW and sky clearness, we calculate $P_{rad}$ by assuming $T_s = T_{amb}$, a solar irradiation of 900 W/m$^2$ and two sky clearness factors of 0.7 and 1.0, respectively. These calculations were done with the spectral properties of a batch of our BaSO$_4$ RC paint, i.e. 3.6% solar absorptance and a sky-window emittance of >95% [22]. The results can be seen in
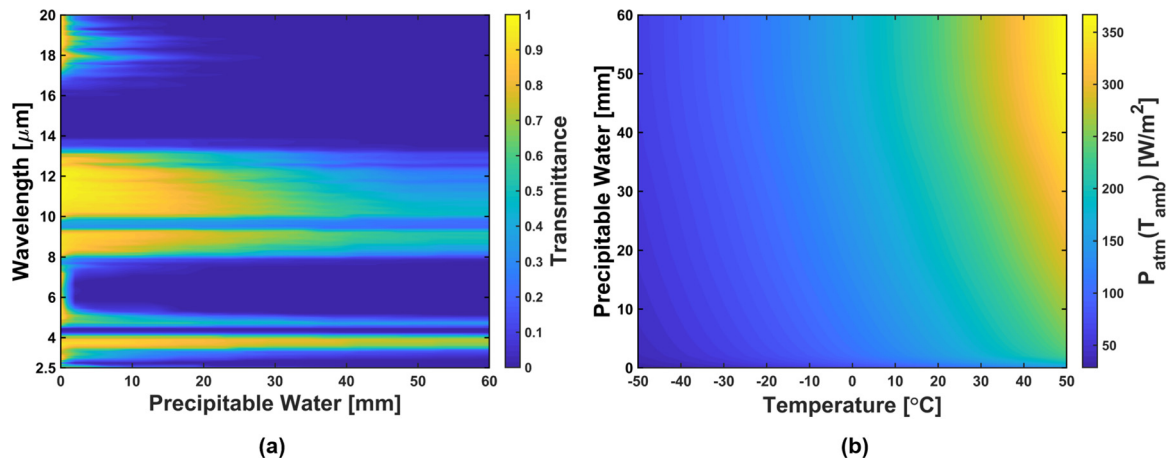
**Fig. 1.** (a) Atmospheric transmittance as a function of wavelength and precipitable water from MODTRAN [37–39]. (b) Atmospheric thermal irradiation dependence on ambient temperature and precipitable water.
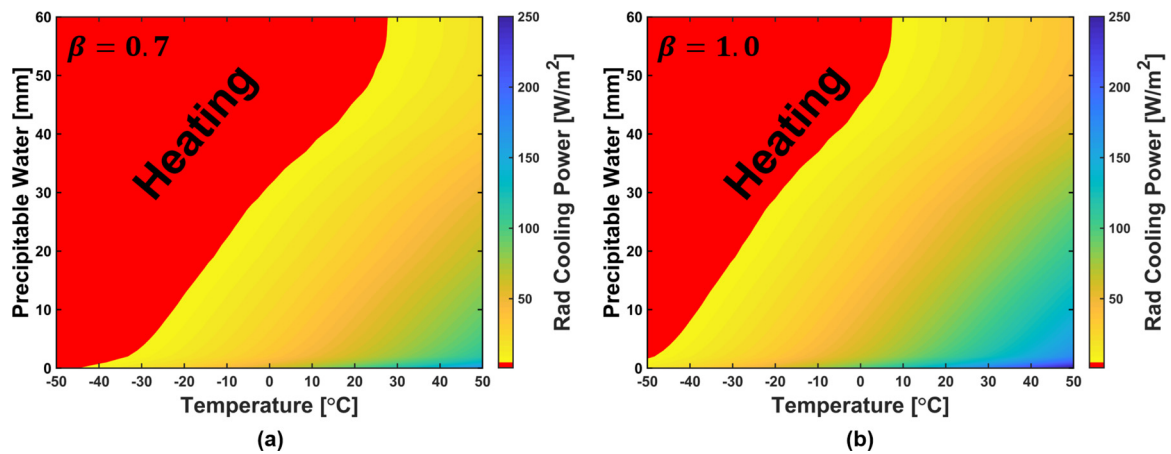


**Fig. 2.** (a) Example net radiative cooling power as a function of precipitable water and temperature for RC paint with the following assumptions, $\beta = 0.7$, $P_{solar} = 900$ W/m$^2$, and $T_s = T_{amb}$. (b) Same example calculation as (a) except $\beta = 1.0$ to illustrate the impact of sky clearness.

Figs. 2a and 2 b, where Fig. 2a has a sky clearness, $\beta = 0.70$ and Fig. 2b is calculated with $\beta = 1.00$.

Fig. 2 a only shows a net cooling effect from the RC paint for slightly more than 50% of the cases; though it should be noted these calculations are conservative as the radiative heat flux between clouds and RC surfaces is not accounted for. However the magnitude of the heat flux between the RC surface and the clouds is negligible compared to the radiative heat flux from the RC surface to deep-space (T = 3 K), due to a small temperature difference between the surface and the clouds. Fig. 2b presents a more positive result that correlates well with works in the literature, which is a clear day, $\beta = 1$, with a low PW yielding cooling powers of 100–150 W/m$^2$. While the cooling power in Fig. 2b shows radiative heat fluxes up to 250 W/m$^2$, it is not a common occurrence as ambient temperatures > 45 °C do not happen often in most United States climates. Moreover, it should be noted that results in Figs. 2a and 2 b only model the radiative heat fluxes, they do not account for the parasitic heat gains from convection or conduction. TRNSYS handles these loads within the program so they do not need to be included in our radiative model [26].

*3.2. Energy savings from radiative cooling*

Utilizing the developed radiative cooling model, a look-up table was constructed, for TRNSYS to interface with, based on the spectral properties of the surface, the solar irradiation, the build-

ing surface temperature, ambient temperature, and PW to give a radiative heat flux on the surface of the building. Then TRNSYS solves for the cooling demand based on the radiative heat flux, dynamic convective load from the wind, infiltration rates, and internal gains. Furthermore, the TRNSYS model accounts for the transient heat conduction through the building envelope, separate conditioned spaces based on room locations, separate treatment for the doors, windows, walls, and floors, as well as internal solar gains through the windows [25,26]. To illustrate the main heat loads in the model, the hourly heat flux data for the typical building type is presented in Figs. 3a (no RC) and 3 b (RC paint) for July 24th in Phoenix, AZ. In the top portions of both Figs. 3a and 3 b, a positive heat flux correlates to energy transfer into the system while a negative heat flux correlates to energy transfer leaving the system.

From the bottom portion of Fig. 3a it can be seen that the south roof surface temperature goes > 10 °C above the ambient temperature due to the solar absorptance. This increase in surface temperature creates a negative convective heat flux as the air would actually be cooling the surface between sunrise and sunset. Results for the RC building, illustrated in Fig. 3b, show the roof temperature consistently staying below the ambient temperature meaning it is able to achieve full 24-hour cooling below ambient. Since the surface temperature is below the ambient temperature, the largest external heat flux in Fig. 3b is the convective heat flux, as it heats the surface. While the cooling heat flux from the below ambient
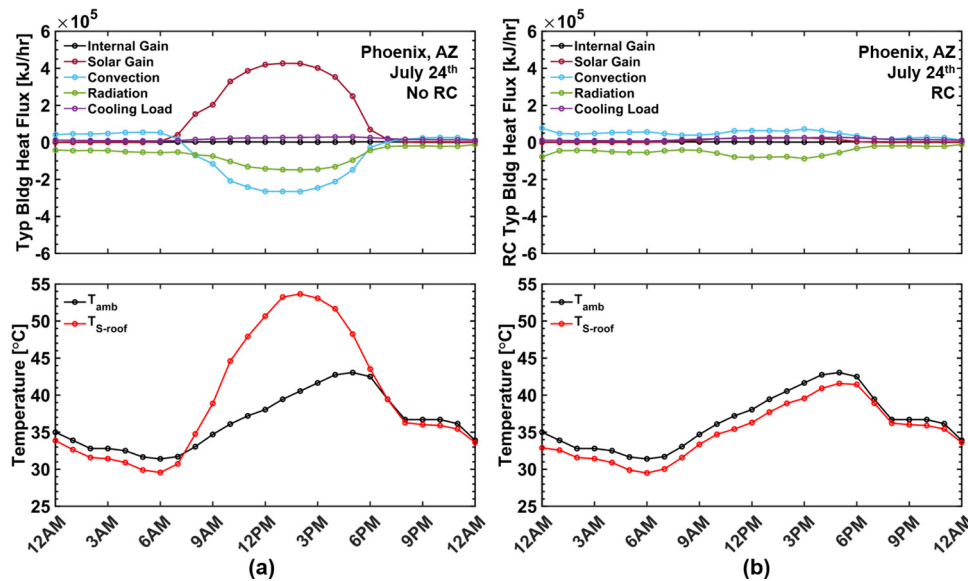
**Fig. 3.** (a) (Top) Hourly heat fluxes for the typical building with no RC, (Bottom) Ambient temperature and south roof temperature from TMY3 data set for Phoenix, AZ on July 24th [33]. (b) (Top) Hourly heat fluxes for the typical building with RC paint. (Bottom) Ambient temperature and south roof temperature from TMY3 data set for Phoenix, AZ on July 24th [33].

exterior surface temperature is partially beneficial to the building envelope, it is not the main contribution to the energy savings. The largest contribution of the RC paint is the offset of the solar gains, diminishing this dominant heat flux takes a large load off the total building cooling demand as the exterior surfaces are not being heated and then conducting that heat to the interior space. Furthermore, we analyze the surface temperature of the RC painted building and see that while it cools below ambient it is still above the thermostat set-point temperature of 23 °C throughout the entire day. Therefore, even with an ultra-efficient radiative cooling surface able of achieving full 24-hour cooling below the ambient temperature, the air-conditioning system still needs to cool the space to maintain the set-point temperature in certain climates with high ambient temperatures.

Using our high fidelity RC building model, we studied the benefits of RC across the United States by simulating the 16 representative cities for each climate zone recommended by the DOE [23]. We considered four cases for each city by varying the building type between typical and high-efficiency, both with and without our RC paint on the buildings. The results of all these simulations are presented in Figs. 4a–d.

Figs. 4 a and 4 b show the electricity usage per unit floor area for an entire cooling season for a typical year for the no RC paint (red) and RC paint (blue) buildings for both the High-Efficiency and Typical building types, respectively. The amount of electricity required to cool the air-conditioned space required for the High-Efficiency Building is lower than the Typical building across all climate zones, which is expected as it has better thermal insulation. While the amount of cooling electricity reduction from the RC paint looks to be uniform across the different cities, Fig. 4c illustrates the impact of the diverse range of climates and how the cooling load reduction from the RC paint is impacted for both building types, High-Efficiency (red) and Typical (blue). The Typical building has greater electricity savings from RC again because the thermal insulation is less. Therefore, when the cooling power from the RC paint cools the surface below the set-point temperature (23 °C) it is more effectively utilized for cooling the interior space. Although Miami, FL has the third largest cooling energy demand, due to its high humidity it only has the sixth largest cooling energy reduction due to the negative PW/humidity effects on RC.

Fig. 4 d presents the cooling percentage electricity savings for each city for both the High-Efficiency (red) and Typical (blue) building types, respectively. The relative cooling electricity savings gives a different perspective to the impact of the RC paint compared to the absolute cooling electricity reduction. For example, Phoenix, AZ has the largest cooling electricity reduction but the second smallest percentage cooling electricity savings; this is due to the large cooling electricity required to maintain the indoor set-point temperature and how far the set-point temperature differs from the ambient temperature. Fig. 3b illustrates this point where even though the RC paint keeps the exterior temperature below the ambient the exterior surface is still > 30 °C for most of the day while the set-point is 23 °C, meaning further cooling is required. This effect explains why the milder, more dry climates in Fig. 4d have the greatest percentage cooling electricity savings from the RC paint. In these climates, the exterior surfaces can be cooled below the set-point temperature and offset a majority of the other cooling loads. However, it should be noted that as long as the ambient temperature is above the set-point, some type of active cooling will be required due to infiltration, internal gains, and latent effects. Fig. 4d also shows that RC can yield large relative savings in northern climate zones due to their low cooling demand. However, the absolute electricity reductions are smaller in the northern climate zones compared to southern zones, since the cooling demand is lower.

Fig. 5 presents the electricity savings of RC on a United States map by ASHRAE climate zone to demonstrate where RC is the most effective [23,32].
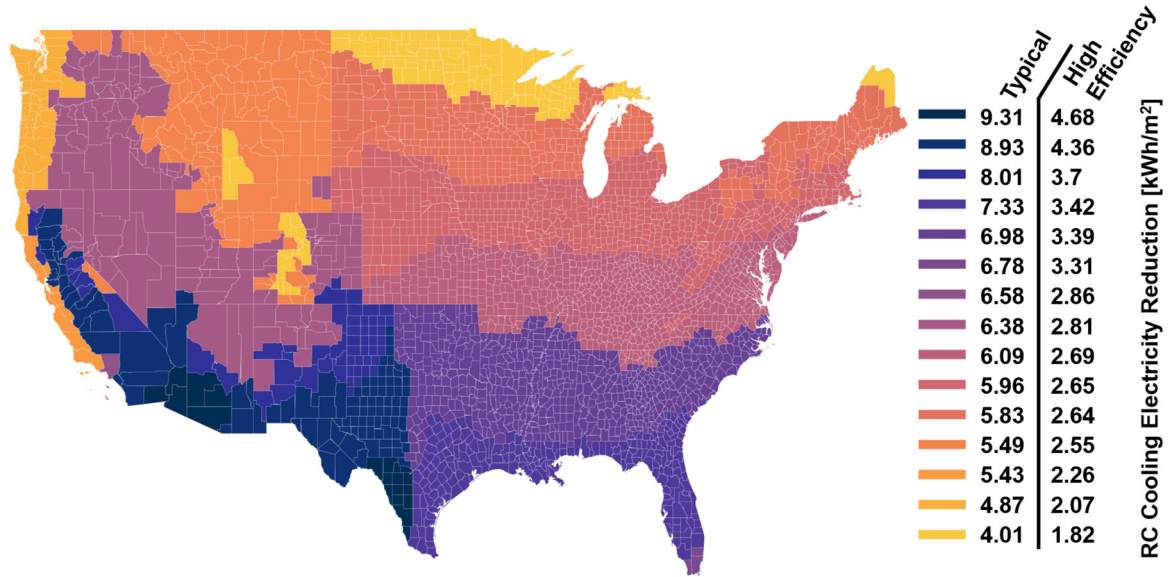
Visualizing the cooling electricity reduction across the United States is the most direct method for seeing the impact of diverse climates on the cooling performance of the RC materials. While this result is specific to RC paints [21,22,29], the geographic trends are applicable for all radiative cooling materials.

## 4. Discussion and conclusion

Our newly developed weather dependent radiative cooling (RC) model for exterior envelope surfaces was integrated into a high-fidelity, single-story residential building model to study the benefits of RC materials across all the climate zones in the United
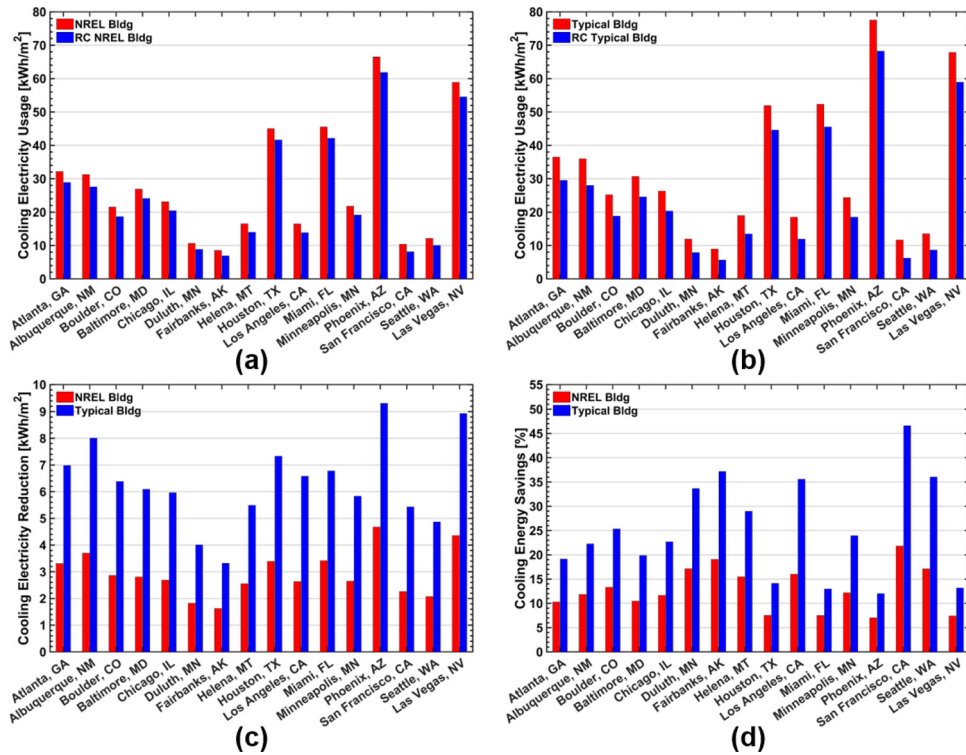
**Fig. 4.** Annual cooling electricity requirement normalized by floor area for the High-Efficiency building (a) and Typical Building (b), both with and without RC paint across 16 cities each with a unique climate. Annual cooling electricity reduction normalized by floor area (c) and percentage electricity savings (d) due to RC paint for the 16 cities for the High-Efficiency building and Typical building types.



**Fig. 5.** Annual cooling electricity reduction normalized by floor area from RC paint across the United States for both the Typical and High-Efficiency building types. This data is generated by running the representative 16 cities recommended by DOE for each ASHRAE climate zone in the United States [23,32].

States. We used the models to illustrate the impact that precipitable water (PW) has on RC surfaces due to its effect on atmospheric transmittance and atmospheric irradiation, as well as integrated the effects of both cloud coverage and wind speed.

The building model was used to shed light on the benefits when a radiative cooling material is utilized as an exterior surface. It was found that the heat flux due to the below ambient temperature of the RC surface is much less important than the reduction of solar gains. There is a subtle difference between the two effects. An exterior coating could have high reflectance in the solar

spectrum and low emittance in the mid-IR and still show similar cooling energy savings. However, the opposite case is not true, an exterior coating could not have high emittance in the mid-IR and poor solar reflectance and show the same benefits. Previous work also illustrated this prioritization when the RC figure of merit was defined, where solar reflectance plays a more important role than the IR emittance [22].

Using DOE's 16 recommended cities, we found that radiative cooling can decrease the cooling electricity requirements by more than 7% and 12% for the High-Efficiency and Typical Build-

ings, respectively [23]. We have shown that RC materials have a greater benefit when they are retrofit onto existing typical buildings that have typical thermal insulation when compared to high efficiency (NREL) buildings with higher thermal insulation in the walls and roof. Well-insulated buildings will see less benefit from RC materials because the "cooling-effect" is not realized in the air-conditioned space. The largest implication of our study is the impact that different climate zones have on RC performance. Fig. 5 clearly illustrates the negative impact that PW has on RC performance. Intuition might suggest that hotter climates would always have greater energy benefits from the radiative cooling effect; however this is not always the case as PW, wind speed, and sky clearness also play important roles in the cooling electricity savings from RC materials. Furthermore, this work motivates the need to incorporate RC materials into more advanced integrated systems to realize the full benefits of the cooling power and increase the electricity savings, such as integrated radiative cooling A/C systems or cold thermal storage methods.

## Declaration of Competing Interest

The authors declare no competing interest with the work presented.

## CRediT authorship contribution statement

**Joseph Peoples:** Conceptualization, Methodology, Writing – original draft, Writing – review & editing. **Yu-Wei Hung:** Conceptualization, Methodology, Writing – original draft, Writing – review & editing. **Ziqi Fang:** Formal analysis, Writing – original draft, Writing – review & editing. **James Braun:** Conceptualization, Supervision, Writing – review & editing. **W. Travis Horton:** Conceptualization, Supervision, Writing – review & editing. **Xiulin Ruan:** Conceptualization, Supervision, Writing – review & editing.

## Acknowledgments

## References

[1] U.S. EIA, Annual energy outlook 2019 with projections to 2050, Annual Energy Outlook 2019 with projections to 2050 44 (8) (2019) 1–64. https://www.eia.gov/outlooks/aeo/pdf/aeo2019.pdf. DOE/EIA-0383(2012) U.S.

[2] R. Family, M.P. Mengüç, Materials for radiative cooling: A Review, Procedia Environ Sci 38 (2017) 752–759, doi:10.1016/j.proenv.2017.03.158. http://linkinghub.elsevier.com/retrieve/pii/S187802961730169X

[3] M. Zeyghami, D.Y. Goswami, E. Stefanakos, A review of clear sky radiative cooling developments and applications in renewable power systems and passive building cooling, Sol. Energy Mater. Sol. Cells 178 (January) (2018) 115–128, doi:10.1016/j.solmat.2018.01.015.

[4] A.K. Goyal, A. Kumar, Recent advances and progresses in photonic devices for passive radiative cooling application : a review, J. Nanophotonics 14 (3) (2020) 1–20, doi:10.1117/1.JNP.14.

[5] E.A. Goldstein, A.P. Raman, S. Fan, Sub-ambient non-evaporative fluid cooling withthesky, Nat. Energy 2 (9) (2017) 17143, doi:10.1038/nenergy.2017.143.

[6] B. Zhao, M. Hu, X. Ao, G. Pei, et al., Conceptual development of a building-integrated photovoltaicradiative cooling system and preliminary performance analysis in eastern china, Appl. Energy 205 (August) (2017) 626–634, doi:10.1016/j.apenergy.2017.08.011.

[7] K. Zhang, D. Zhao, X. Yin, R. Yang, G. Tan, et al., Energy saving and economic analysis of a new hybrid radiative cooling system for single-family houses in the USA, Appl. Energy 224 (April) (2018) 371–381, doi:10.1016/j.apenergy.2018.04.115.

[8] J. Peoples, Y.-W. Hung, X. Li, D. Gallagher, N. Fruehe, A. Yuksel, J. Braun, T. Horton, X. Ruan, et al., Concentrated radiative cooling, Appl Energy 310 (11838) (2022) 1–7, doi:10.1016/j.apenergy.2021.118368. http://arxiv.org/abs/2010.02426

[9] Z. Yi, Y. Lv, D. Xu, J. Xu, H. Qian, D. Zhao, R. Yang, et al., Energy saving analysis of a transparent radiative cooling film for buildings with roof glazing, Energy and Built Environment 2 (2) (2021) 214–222, doi:10.1016/j.enbenv.2020.07.003.

[10] R. Lamba, M. Zeyghami, D. Young, D.Y. Goswami, S.C. Kaushik, et al., Thermal Modeling of a Building Integrated Radiative Cooler for Space Cooling Applications, in: IMECE 2018, 2018, pp. 1–6, doi:10.1115/imece2018-87456.

[11] M. Wei, W. Wu, D. Li, H. Xu, Y. Lu, W. Song, et al., Universal strategy for all-weather and all-terrain radiative cooling with non-reciprocal mid-infrared windows, Sol. Energy 207 (July) (2020) 471–478, doi:10.1016/j.solener.2020.07.010.

[12] Y. Liu, A. Bai, Z. Fang, Y. Ni, C. Lu, Z. Xu, et al., A pragmatic bilayer selective emitter for efficient radiative cooling under direct sunlight, Materials (Basel) 12 (8) (2019), doi:10.3390/ma12081208.

[13] T. Li, Y. Zhai, S. He, W. Gan, Z. Wei, M. Heidarinejad, D. Dalgo, R. Mi, X. Zhao, J. Song, J. Dai, C. Chen, A. Aili, A. Vellore, A. Martini, R. Yang, J. Srebric, X. Yin, L. Hu, et al., A radiative cooling structural material, Science 364 (6442) (2019) 760–763, doi:10.1126/science.aau9101.

[14] Y. Tian, H. Shao, X. Liu, F. Chen, Y. Li, C. Tang, Y. Zheng, et al., Superhydrophobic and recyclable cellulose-fiber-based composites for high-Efficiency passive radiative cooling, ACS Appl. Mater. Interfaces 13 (19) (2021) 22521–22530, doi:10.1021/acsami.1c04046.

[15] Y. Tian, X. Liu, Z. Wang, J. Li, Y. Mu, S. Zhou, F. Chen, M.L. Minus, G. Xiao, Y. Zheng, et al., Subambient daytime cooling enabled by hierarchically architected all-inorganic metapaper with enhanced thermal dissipation, Nano Energy 96 (September 2021) (2022) 107085, doi:10.1016/j.nanoen.2022.107085.

[16] Y. Tian, X. Liu, J. Li, A. Caratenuto, S. Zhou, Y. Deng, G. Xiao, M.L. Minus, Y. Zheng, et al., Scalable, fire-retardant, and spectrally robust melamine-formaldehyde photonic bulk for efficient daytime radiative cooling, Applied Materials Today 24 (2021) 101103, doi:10.1016/j.apmt.2021.101103.

[17] Z. Huang, X. Ruan, Nanoparticle embedded double-layer coating for daytime radiative cooling, Int. J. Heat Mass Transf. 104 (2017) 890–896, doi:10.1016/j.ijheatmasstransfer.2016.08.009.

[18] J. Peoples, X. Li, Y. Lv, J. Qiu, Z. Huang, X. Ruan, et al., A strategy of hierarchical particle sizes in nanoparticle composite for enhancing solar reflection, Int. J. Heat Mass Transf. 131 (2019) 487–494, doi:10.1016/j.ijheatmasstransfer.2018.11.059.

[19] J. Mandal, Y. Yang, N. Yu, A.P. Raman, et al., Paints as a scalable and effective radiative cooling technology for buildings, Joule 4 (7) (2020) 1350–1356, doi:10.1016/j.joule.2020.04.010.

[20] X. Ruan, X. Li, Z. Huang, J. Peoples, Metal-Free Solar-Reflective Infrared-Emissive Paints and Methods of Producing the Same, PCT/US2019/054566, 2019, https://patentscope.wipo.int/search/en/detail.jsf?docId=WO2020072818&tab=PCTBIBLIO.

[21] X. Li, J. Peoples, Z. Huang, Z. Zhao, J. Qiu, X. Ruan, et al., Full daytime sub-Ambient radiative cooling in commercial-like paints with high figure of merit, Cell Rep. Phys. Sci. 1 (10) (2020) 100221, doi:10.2139/ssrn.3652325.

[22] X. Li, J. Peoples, Y. Peiyan, X. Ruan, et al., Ultrawhite baSO4 paints and films for remarkable daytime subambient radiative cooling, ACS Appl. Mater. Interfaces 13 (18) (2021) 21733–21739, doi:10.1021/acsami.1c02368.

[23] E.E. Office, R. Energy, Commercial Reference Buildings, 2020 https://www.energy.gov/eere/buildings/commercial-reference-buildings.

[24] M.W. Smith, Analysis of the thermal performance of tierra ia low-Energy high-mass residence, Energy Build 33 (7) (2001). http://www.nrel.gov/docs/fy01osti/25873.pdf

[25] S. Holloway, An Annual Performance Comparison of Various Heat Pumps in Residential Applications, Purdue University, 2013 Masters of science.

[26] S.A. Klein, E. al., TRNSYS 18: A Transient System Simulation Program, 2017,

[27] ASHRAE, 90.2–2018 Energy-efficient design of low-Rise residential buildings, ANSI/ASHRAE/IES Standard (2018).

[28] ASHRAE, 62.2–2019 Ventilation and Acceptable Indoor Air Quality in Residential Buildings, ANSI/ASHRAE Standard (2019).

[29] J. Mandal, Y. Fu, A. Overvig, M. Jia, K. Sun, N. Shi, H. Zhou, X. Xiao, N. Yu, Y. Yang, et al., Hierarchically porous polymer coatings for highly efficient passive daytime radiative cooling 9513 (September) (2018) 1–9, doi:10.1126/science.aat9513.

[30] Y. Cengel and Ghajar, Afshin, Heat and Mass Transfer: Fundamentals and Applications, 4th, McGraw-Hill, New York, 2011.

[31] Engineering-Toolbox, Convective Heat Transfer, 2003, https://www.engineeringtoolbox.com/convective-heat-transfer-d_430.html.

[32] M.C. Baechler, T.L. Gilbride, P.C. Cole, M.G. Hefty, K. Ruiz, Guide to determining climate regions by county, Pacific Northwest National Laboratory and Oak Ridge National Laboratory 7 (August) (2015) 1–34. https://www.energy.gov/sites/prod/files/2015/10/f27/ba_climate_region_guide_7.3.pdf

[33] S. Wilcox, W. Marion, User's Manual for TMY3 Data Sets, Technical Report, National Renewable Energy Laboratory., Golden, Colorado, 2008. NREL/TP-581-43156

[34] B. Wozniak, J. Dera, Light absorption by water molecules and inorganic substances dissolved in sea water, in: Light Absorption in Sea Water, volume 33, Springer US, New York, 2007, pp. 11–81, doi:10.1007/978-0-387-49560-6_2.

[35] M.F. Modest, Radiative heat transfer, Elsevier Science, 2013.

[36] J.R. Howell, R. Siegel, M.P. Menguc, Thermal radiation heat transfer, CRC Press, Boca Raton, FL, 2016.

[37] A. Berk, P. Conforti, R. Kennett, T. Perkins, F. Hawes, J. van den Bosch, et al., MODTRAN6: a major upgrade of the MODTRAN radiative transfer code, Algorithms and Technologies for Multispectral, Hyperspectral, and Ultraspectral Imagery XX 9088 (June 2014) (2014) 90880H, doi:10.1117/12.2050433.

[38] A. Berk, P. Conforti, F. Hawes, An accelerated line-by-line option for MODTRAN combining on-the-fly generation of line center absorption within 0.1 cm-1 bins and pre-computed line tails, Algorithms and Technologies for Multispectral,

Hyperspectral, and Ultraspectral Imagery XXI 9472 (May 2015) (2015) 947217, doi:10.1117/12.2177444.

[39] S.S. Inc, MODTRAN Web App, 2016, http://modtran.spectral.com/modtran_home.

[40] V. Menoux, R. Le Doucen, C. Boulet, A. Roblin, A.M. Bouchardy, et al., Collision induced absorption in the fundamental band of N2 temperature dependence of the absorption for N2 N2 and N2 O2 pairs, Appl. Opt. 32 (3) (1993) 263, doi:10.1364/ao.32.000263.

[41] E.D. Jansen, T.G. van Leeuwen, M. Motamedi, C. Borst, A.J. Welch, et al., Temperature dependence of the absorption coefficient of water for midinfrared laser radiation, Lasers Surg Med 14 (3) (1994) 258–268, doi:10.1002/lsm.1900140308.

[42] J.M. Theriault, P.L. Roney, F. Reid, A. Kohnle, et al., Temperature dependence of atmospheric transmittance in the 2.8-5.5 um region, Propagation Engineering 1115 (October 1989) (1989) 295, doi:10.1117/12.960882.

[43] J.A. Lane, Far-infrared spectrum of liquid water, J. Opt. Soc. Am. 56 (10) (1966) 1398, doi:10.1364/josa.56.001398.